

# Hydroprinted Liquid-Alloy-Based Morphing Electronics for Fast-Growing/Tender Plants: From Physiology Monitoring to Habit Manipulation

Jiajun Jiang, Shuo Zhang, Bei Wang, Han Ding, and Zhigang Wu\*

Monitoring physiological signals and manipulating growth habits of living plants in real time are important for botany research, biohybrid plant robots, and precision agriculture. Although emerging epidermal electronics that can conveniently acquire vital signals of living organisms exhibit a high potential for such scenarios, it is a significant challenge to adapt such devices for plants, because they are fragile and usually have complex surfaces that can change significantly during rapid growth. A gentle fabrication process is critical in order to employ compliant electronic systems to adapt to this highly dynamic situation. In this study, a hydroprinted liquid-alloy-based morphing electronics (LAME) process is employed for fast-growing plants that will sense physiological signals and even function as a biohybrid to determine plant behavior on demand. Besides various surfaces of inorganic targeting substrates, pinning liquid alloy circuits onto the complex plant epidermis is enhanced by introducing high-surface-energy liquid. Functionally, the new developed LAME can be used to monitor leaf moisture content and length, and manipulate leaf and bean sprout orientation. This study lays the foundation for a new form of morphing electronics for botany or biohybrid plant robots, potentially impacting the next generation of precision agriculture and smart hybrid robots.

nanomaterials into plant cells and vascular systems of seedlings and mature plants to impact the intrinsic properties related to photosynthesis;<sup>[8]</sup> conversion of native plant ATP to chemiluminescence for indirect lighting;<sup>[9]</sup> measurement of plant electrical signals to predict the characteristics of input light stimuli;<sup>[10]</sup> patterning of graphene-based nanomaterials to detect the relative water humidity on the surface of leaves;<sup>[11]</sup> deposited thin gold polydimethylsiloxane (PDMS) films as plant wearables for localized microclimate and growth monitoring;<sup>[12]</sup> creation of a triboelectric mechanism to harvest environmental mechanical energy;<sup>[13,14]</sup> and integration of digital circuits on plants to produce plant–robot hybrids.<sup>[7]</sup>

Epidermal electronics to interface electronics to living mammalian cells, tissues, and organs has advanced rapidly in recent years, offering new opportunities to vital physiological signal monitoring.<sup>[15–17]</sup> Various strategies have been devised based on the materials and structural design of elec-

tronic components and target substrates.<sup>[18,19]</sup> Reported applications to living organisms include electroencephalogram and electrocardiogram recording,<sup>[15]</sup> as well as temperature,<sup>[16,20,21]</sup> blood pressure,<sup>[22,23]</sup> blood oxygen,<sup>[24]</sup> blood glucose,<sup>[25,26]</sup> surface electromyography,<sup>[27]</sup> and motion<sup>[28–30]</sup> monitoring. Also, artificial electronic skin with biosignal monitoring<sup>[31–35]</sup> and haptic interfaces<sup>[36]</sup> have been developed. For precise monitoring of plant growth, it is straightforward to adapt current epidermal electronics to plant electronics by patterning graphene-based nanomaterials on the surface of the leaf<sup>[11]</sup> and vapor-printing polymer films directly onto living plants.<sup>[37]</sup> Further, new electronics can morphologically adapt to highly dynamic situations,<sup>[38–40]</sup> without hindering the plant growth. Hence, these devices could be a desirable candidate for plant behavior manipulation or to create plant–robot hybrids.


There are several looming challenges to integrate such morphing electronics with epidermis of living plants. First, many plants are too vulnerable and fragile to withstand external stimuli, such as mechanical pressure or stress, heat flux, or toxic chemical vapors which means that the fabrication process must be gentle and not introduce potential toxic substances. Second, because plants change their morphology during rapid growth and development, epidermal electronic circuits should

## 1. Introduction

Monitoring and manipulating growth, health, and other behavior of plants is providing practical and precise approaches for crop management,<sup>[1]</sup> horticulture,<sup>[2]</sup> and smart plant sensors.<sup>[3,4]</sup> It is of great significance to synthesize and integrate bioinspired transducers with the goal of creating biohybrid smart systems and robots.<sup>[5–7]</sup> Work has been done from various perspectives including introduction of functional

J. Jiang, S. Zhang, B. Wang, Prof. H. Ding, Prof. Z. G. Wu  
State Key Laboratory of Digital Manufacturing Equipment  
and Technology  
School of Mechanical Science and Engineering  
Huazhong University of Science and Technology  
Wuhan 430074, China  
E-mail: zgwu@hust.edu.cn

B. Wang  
Department of Material Science and Engineering  
Uppsala University  
Box 534, Uppsala 75121, Sweden

 The ORCID identification number(s) for the author(s) of this article can be found under <https://doi.org/10.1002/smll.202003833>.

DOI: 10.1002/smll.202003833

be intrinsically stretchable and capable of undergoing morphological change. Third, since the surface of the plant epidermis is complex on the micro- and nanoscales,<sup>[41,42]</sup> conformable attachment techniques for such morphologies need to be developed. However, current technologies cannot meet all the three challenges at the same time.

Gallium-based liquid alloy (LA), a low toxic liquid alloy with intrinsically high fluidity and electrical conductivity,<sup>[43–46]</sup> is tolerated by living plants and can easily accommodate the morphologically complex epidermal surfaces upon attachment. Thus, a smart system based on liquid-alloy-based morphing electronics (LAME) could provide an excellent solution for living plant monitoring and behavior manipulation. Previously, many approaches have been proposed to fabricate LA circuits on 3D surfaces,<sup>[47–49]</sup> including direct printing,<sup>[50,51]</sup> roller pen printing,<sup>[52,53]</sup> masked printing,<sup>[54,55]</sup> atomized printing,<sup>[56]</sup> direct 3D printing,<sup>[57–59]</sup> and flexographic printing.<sup>[60]</sup> However, these approaches often rely on external applied pressure which is overly harsh for fragile plants. In addition, the complex micro- and nanoscale surface of the plant epidermis often leads to weakened interfacial adhesion to the liquid alloy, severely decreasing the device success rate. Hydroprinting, or water transfer printing, is a gentle surface patterning technology widely used in the decorative coating industry and recently has been developed to provide accurate mapping between designed 2D patterns to targeting 3D surface.<sup>[61]</sup> Most recently, it has been used to transfer curved circuits, such as aluminum ribbons,<sup>[62,63]</sup> silver-nanoparticle-based ink,<sup>[64,65]</sup> and graphene.<sup>[11,66]</sup> Also, with particle-assisted sticking, thin Ag–In–Ga E-Skins has been hydroprinted on carrier films.<sup>[67]</sup> However, such circuits or carrier film are almost solid and cannot morph to accommodate the rapid growth of plants; this may result in long-term stress, hindering the growth of the plants or cracking of the devices themselves.

Using an innovative, gentle hydroprinting of LA circuits on the fragile plant epidermis, we have developed an intrinsically plant morphing electronics—LAME—in which functional LA circuits with morphing ability can be conformable transferred onto the surfaces of plants without carrier films. Such LAME circuits function well on the epidermis of fast-growing (up to 2.3 mm h<sup>−1</sup>) plants for various applications including monitoring the moisture content of lilies and roses, monitoring the length of sprout hypocotyls, and manipulating the growth of sprouts (intertwine a ladder; Video S1, Supporting Information).

## 2. Results and Discussion

The step-by-step process for hydroprinting LAME on living plants (bean sprout as an example) is illustrated in **Figure 1A** and complementary details in **Figure 1B**. i) Using a previously developed process,<sup>[56]</sup> a prepatterned LA circuit (see fabrication details in **Figure S1** in the Supporting Information) on a water-soluble polyvinyl alcohol (PVA) film is placed on the surface of water and then swollen as a layer of soft and viscous PVA gel. ii) For targeting seedlings, epidermises can be categorized into LA-stuck and LA-unstuck depending on their behavior on LA; LA can be pinned on the former, such as a sprout, directly via the LA oxide layer, whereas on the latter, such as rose and

lily petals, the LA droplet is unstable and mobile due to weak interfacial interaction. iii) The prepared growing seedling is aligned toward the LA circuit and dipped into water whereby the LA circuit on the PVA gel is transferred and attached onto the plant epidermis due to surface tension and hydrostatic pressure during the immersion process (more details are given in **Figure S2** in the Supporting Information). iv) After being slowly pulled out of water, the seedling is encapsulated within a thin layer of swollen PVA gel. The LAME is completely adhered to the LA-stuck epidermis while the LAME partially adhered to the LA-unstuck epidermis because air remains in the gaps between the device and epidermal surface of the plant. The encapsulating swollen PVA gel maintains the shape and position of LA on LA-unstuck epidermis. v) To remove the residual PVA gel, the seedling is immersed in pure water again. During this process, the water–PVA solution fills the gaps between LA and epidermal surface acting as a temporary bond for the LA. vi) After drying, the water in gaps evaporates and is partly absorbed by the plant. This drives complete and conformal adhesion between the LA and the epidermal surface. vii) Finally, by further integrating other functional components, the growth and growth behavior can be monitored or manipulated via the LAME attached to the plant epidermis. A visual demonstration of the hydroprinting process is provided in **Video S2** (Supporting Information).

An intermediate state of a serpentine LA line on the epidermis of a fast-growing bean sprout hypocotyl (LA-stuck surface, the fastest measured growth rate of 2.3 mm h<sup>−1</sup>) is shown in **Figure 1C**. As shown in **Figure 1D**, a liquid alloy QR code pattern is conformably printed on the surface of a separated red rose petal and on a living rose (LA-unstuck surface). A functional circuit lighting a green light-emitting diode (LED) on a separated rose petal keeps working even after dehydration (**Figure 1E**; more details in **Figure S3** in the Supporting Information). These results indicate that the hydroprinted LAME can be conformably printed not only on LA-stuck but also on LA-unstuck plant epidermises and adjust to the development of plant epidermises undergoing rapid transformations. Furthermore, by printing LAME on a growing bean sprout, sprout growth and “crawling” along a custom-made ladder in a dark container could be manipulated through controlled phototropism enabled by LED emission (**Figure 1F**).

Previous studies have reported that the LA oxide layer plays a crucial role in pinning LA circuits on surfaces with different morphologies,<sup>[43,44,60,68]</sup> and the oxide layer can also mechanically stabilize liquid alloy in stable, nonequilibrium shapes.<sup>[57,69]</sup> However, rough surfaces with complex topography on the micro- and nanoscales, such as rose petals, usually have a lower surface energy and hence do not adhere well to LA, which prevents printed LA circuits from being transferred to them. As shown in **Figure 2A**, we measured the contact angles (advancing contact angle,  $\theta_a$ ; static contact angle,  $\theta_s$ ; and receding contact angle,  $\theta_r$ ) of LA droplets on several surfaces of plants (e.g., sprout cotyledon, sprout hypocotyl, white lily petal, pink rose petal, red rose petal, and champagne rose petal) in air. All of these surfaces exhibit “LA phobicity” ( $\theta_s > 140^\circ$ ). LA droplets are pinned on sprout cotyledon and hypocotyl having a large  $\theta_a$  but a small  $\theta_r$ . However, for the other four plants, slightly different  $\theta_a$  and  $\theta_r$  values were observed. The energy for removing LA

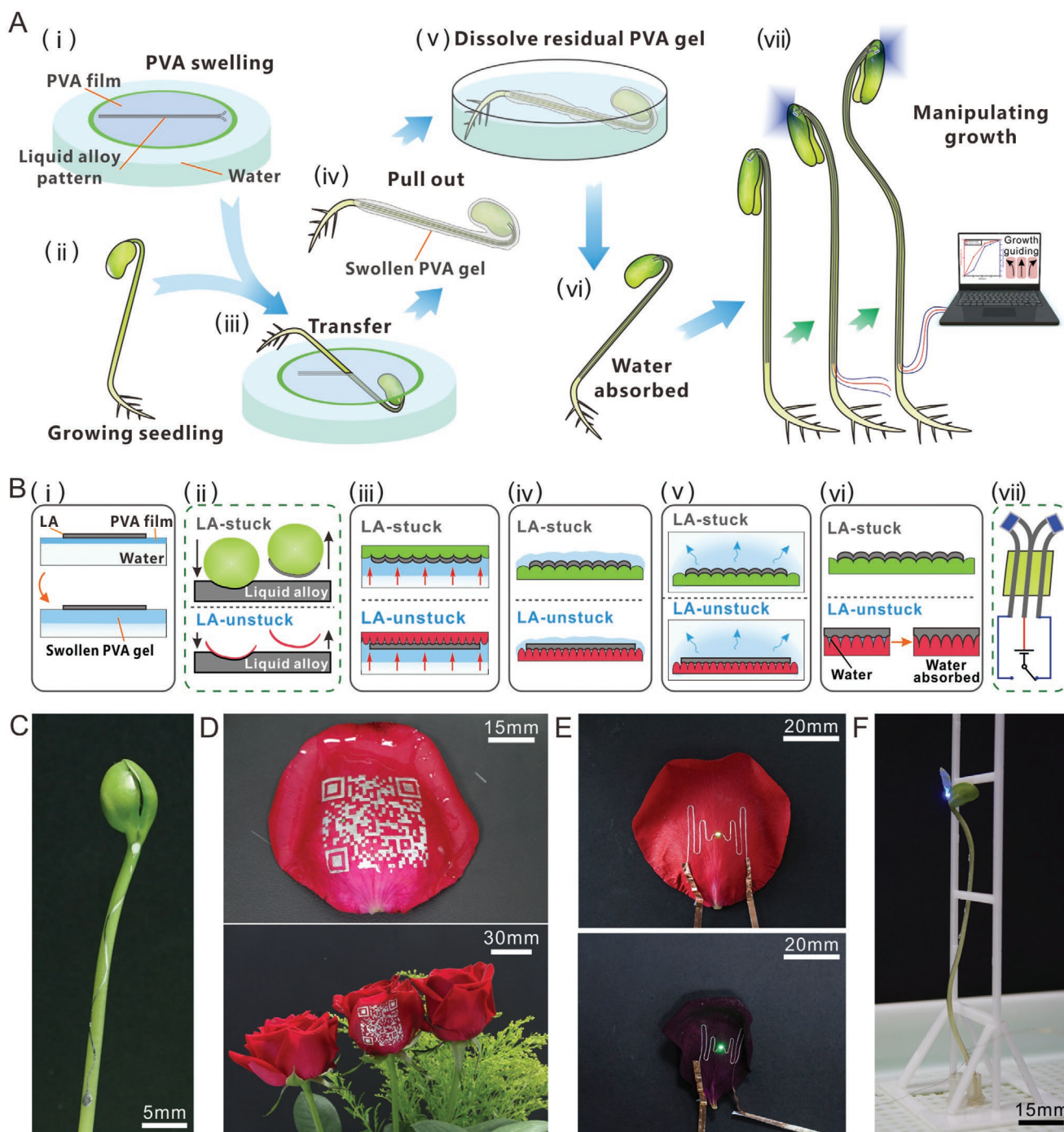


**Figure 1.** Hydroprinting liquid-alloy-based morphing electronics on plants. A) Overview illustration of the process for hydroprinting LAME on living plant epidermises using bean sprouts as an example. B) Complementary details of the fabrication process (see the text for further description of steps): i) PVA swelling process; ii) behavior of LA-stuck and LA-unstuck plants when contacting with LA; iii) transferring LA; iv) PVA gel remaining on the plant; v) PVA gel dissolution; vi) water vaporized or absorbed; and vii) diagram for the guiding LED circuit. C) A sinuous length sensor of  $\approx 500 \mu\text{m}$  width on a living bean sprout seedling. D) Quick response codes printed on roses. E) An LED-LA circuit of  $\approx 400 \mu\text{m}$  width on the rose petal dehydrating from fresh to withered. F) An LED-LA circuit morphing with the growth of the living bean sprout seedling. Selective manipulation of the growth of bean sprouts seedling to "climb" a ladder using LED emission on both sides of the sprout.

( $E_p$ , detailed calculation in the Supporting Information) from sprout is at least four times larger than that from lily and rose (Figure 2B). A large difference between  $\theta_a$  and  $\theta_r$  suggests good adhesion between LA and the epidermal surface according to

a previous study.<sup>[60]</sup> These results indicate that LA will not be well pinned or adhered to the pristine surfaces of lily and rose due to their surface morphologies (Figure S4, Supporting Information). This characteristic can also be observed in pristine



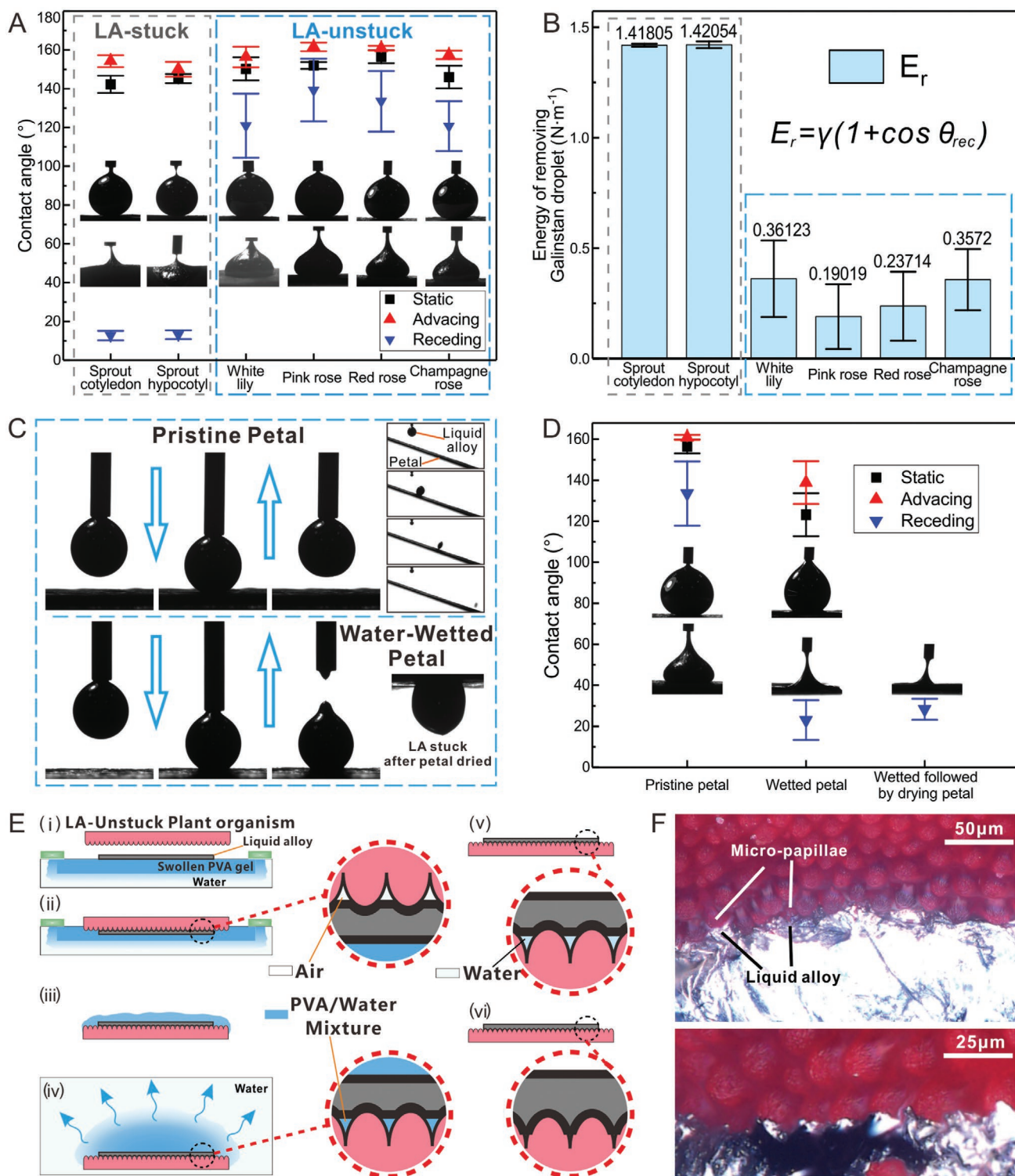


**Figure 2.** Principles of LA adherence to plant epidermis. A) Contact angles (advancing angle, static angle, and receding angle) of LA droplets ( $\approx 4 \mu\text{L}$ ) on different plant surfaces. Gray frame is for LA-stuck surfaces while the blue frame is for the LA-unstuck surfaces. Upper and lower photos show the advancing angles and the receding angles, respectively. B) Calculated surface energy of removing LA droplet from various surfaces. C) Comparison of LA behaviors on pristine and water-wetted rose petals. The upper inset on the right shows the LA droplet contacting and rolling along the petal surface. The lower inset on the right shows the LA droplet pinned on the petal surface after wetting it and subsequent drying. D) Contact angles (advancing angle, static angle, and receding angle) of an LA droplet ( $\approx 4 \mu\text{L}$ ) on a rose petal in different states (pristine, wetted, and wetted followed by drying). E–i–v) Schematic illustration of the process of adhering LA to an unstuckable plant epidermis (see the text for a detailed description). F) Magnified images of a rose petal on which a printed liquid alloy pattern has been printed.



rose petals that these petals are very LA-phobic in air (upper left illustration in Figure 2C). It results in unstable positioning and rolling of the LA droplet on the petal surface (upper right illustration in Figure 2C).

Surprisingly, in some experiments, LAME can be well pinned on lily and rose petals during the hydroprinting process. After careful investigation, we concluded that the introduction of a high-surface-energy liquid like water enables LA to pin onto the rough epidermal surface of flower petals (Figure S4, Supporting Information), finally conformally attaching to the surface. As shown in Figure 2C,D, LA droplets can be pinned and stuck on rose petals by sticking and wetting them with a water/PVA solution (more details are provided in Figure S5 and Video S2 in the Supporting Information). By reversing the position of the droplet, LA still strongly stick on the petal surface even after being dried (lower right illustration in Figure 2C). As shown in Figure 2D,  $\theta_c$  is decreased to  $\approx 23^\circ$  on the wetted petal. These data indicate that the introduction of water assists in pinning LA onto living rose and lily petals. In addition, LA still sticks well on dried petals for which  $\theta_c$  is  $\approx 28^\circ$ .

To better understand the mechanism whereby the liquid alloy pins on diverse surfaces, we schematized the pinning and the subsequent sticking processes in Figure 2E and in Figure S6A (Supporting Information). For LA-stuck surfaces such as sprout cotyledon and hypocotyl, LA circuits can be transferred onto them by dipping them into the swollen PVA solution under surface tension and hydrostatic pressure. The LAME is conformably printed on the surface after being dried (the details and microviews of the LA circuits are given in Figure S6A in the Supporting Information). By contrast, for the LA-unstuck plants with generally complex surfaces, like lily and rose petals, LA circuits behave differently during the hydroprinting process (Figure 2E). Initially, when LA circuits on the PVA film are placed on the water surface, the PVA is swollen, followed by the formation of a soft and viscous PVA gel, which can still support the LA circuits on its surface (Figure 2E-i). Such a viscous gel can wrap LA circuits onto the plant epidermis, although there are still air gaps at the interface of the LA and epidermal surface (Figure 2E-ii,iii). Due to the high osmolarity of the viscous PVA gel/solution, water enters the gel and is pinned to the plant epidermis, consequently leading to a higher energy surface (bottom part of Figure 2C) and hence a stronger bonding between LA and plant epidermis. Then the gaps are continuously filled with PVA solution during the dissolving process, and finally with almost pure water in the gaps (Figure 2E-iv,v). Upon removal from the water bath and drying, the remaining water evaporates or is absorbed by the plant with result that the LAME conformally morphs to the plant epidermis (Figure 2E-vi). Optical photos of LA on the rose petal are shown in Figure 2F. The LA wraps around the micropapillae of the petal can be observed in the magnified panels of Figure 2F, indicating that the LAME is conformally attached to the rose petal. In addition, our experiments also suggest that variation of PVA content (by weight) shows little influence on LA pinning (Figures S5 and S6B and Video S2, Supporting Information).

To further evaluate the hydroprinting process, we investigated LAME attached to various inorganic substrates in terms of patterning capability and mechanical and electrical properties. First, the length and width of designed and processed LA

lines are shown in Figure 3A,B (additional details are given in Figure S7 in the Supporting Information). Although the experimental width and length of LA lines are slightly larger than the designed ones that originated from the UV laser-ablated masked patterning, the LA lines preserve nearly the original size (within 5%) after being transferred. In addition, the spacing between adjacent hydroprinted LA lines becomes larger with decreasing bending (immersing) angles of the substrates (Figure 3C). The elongation of the softened and dissolved PVA film is strongly dependent on the immersing angles. The thicknesses of LA lines before (on PVA) and after hydroprinting (on silicone) are shown in Figure 3D. The changes in length and width, as well as the consumption of LA during the dissolution of residual PVA, lead to the decrease in thickness.

Next, the electrical properties of printed LA circuits were measured and results are shown in Figure 3E and in Figure S8A,B (Supporting Information). Due to the stretching of the swollen PVA film during the hydroprinting process, the resistances of transfer-printed LA lines are somewhat higher than those of the prepatterned ones. The cycling test indicates that the circuits remain functional after stretching 10 000 times under 50% strain and bending 4000 times over  $180^\circ$ , respectively (Figure S8A,B, Supporting Information). Owing to the excellent compliance of swollen PVA gels, LA patterns can be hydroprinted onto various complex 3D surfaces. As shown in Figure 3F, line arrays of varied widths and spacing were hydroprinted on the surface of silicone hemisphere. A line as narrow as  $\approx 70\ \mu\text{m}$  (right upper microview in Figure 3F) and spacing as close as  $\approx 100\ \mu\text{m}$  (right lower microview in Figure 3F) have been achieved. Such resolution depends on the machining accuracy of the predefined patterning techniques that could be improved in the future. The technique is also suited for printing a pattern with varied widths such as the fractal pattern shown in Figure 3G.

Complex 2D patterns can be obtained and transferred to smooth 3D surfaces. As shown in Figure 3H, a  $6\ \text{mm} \times 6\ \text{mm}$  array of liquid alloy squares can be printed on the slope of a silicone hemisphere. An annulus pattern and a polyline can also be printed on the hemisphere (Figure 3I,J). The angles of patterns are kept consistent before and after hydroprinting (Figure S8C, Supporting Information). Furthermore, our process can also be applied to a curvature-discontinuous surface. For instance, a helical, high-fidelity LA-LED circuit was printed on a 3D nondevelopable surface with corrugated wrinkles, including positive and negative Gaussian curvatures (Figure 3K; Video S3, Supporting Information).

The water used in the process offers new opportunities for advanced patterning because of its high fluidity. For instance, as shown in Figure 3L, by dividing the patterns into two or more parts and adopting sequential hydroprinting, a  $360^\circ$  pattern can be created on a surrounding surface. It also makes it possible to print a functional LAME on a double-sided thin polyethylene terephthalate (PET) film ( $100\ \mu\text{m}$ ) without breaking, as illustrated in Figure 3M. Thus, our liquid alloy printing technique enables printing multilayer circuits in one process. More importantly, it offers the ability to print circuits on curved internal surfaces in a confined space which is very difficult to achieve with other current methods. For instance, as shown in Figure 3N, an HUST logo was printed on the inner wall of an

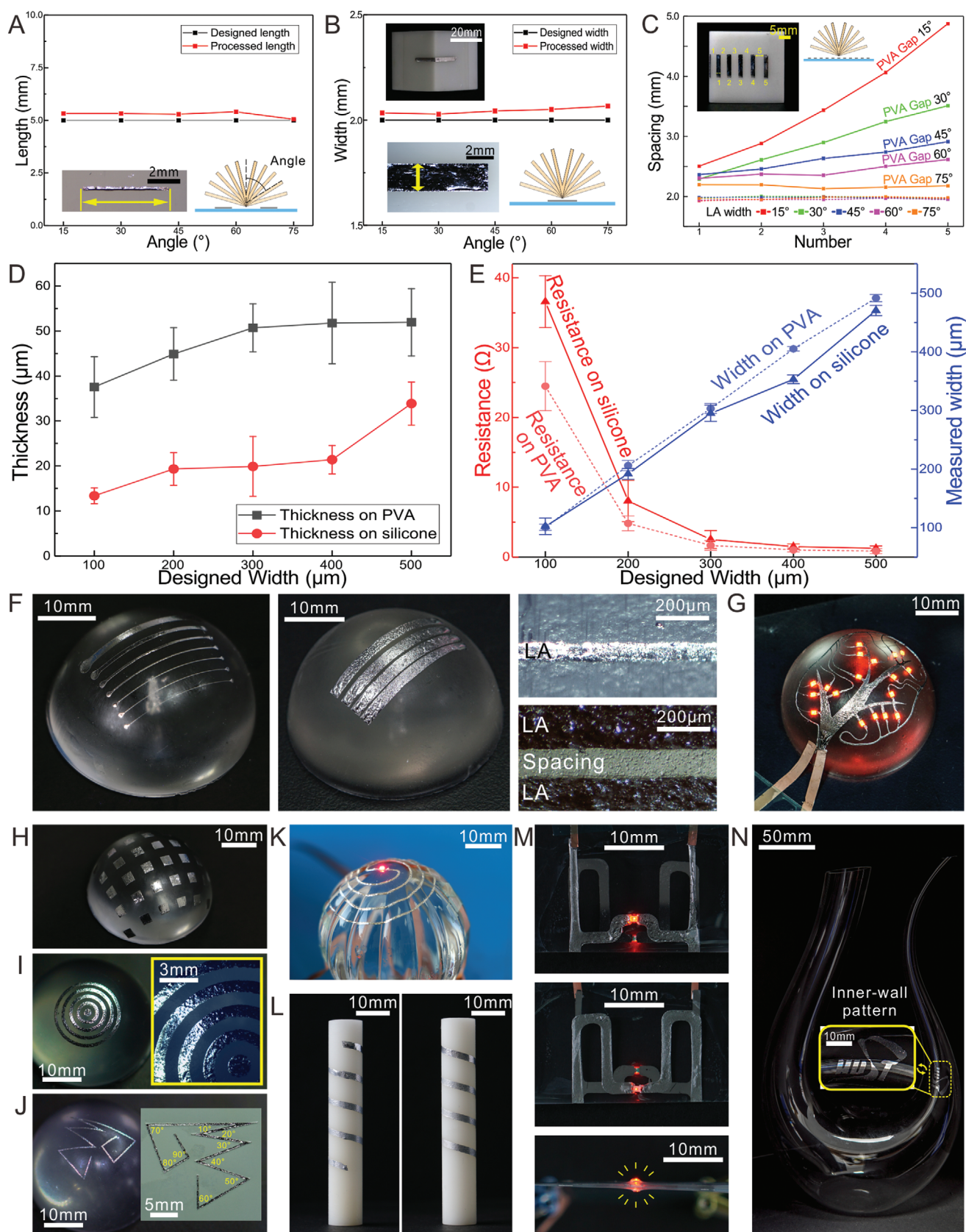


**Figure 3.** Hydroprinting patterning capacity and characterization. A) Designed and measured lengths of LA lines with respect to angle of line deposited on substrates. The inset is an optical photo of an LA line on target substrate. B) Designed and measured width of LA ribbon on target structures.

Amadeo Fatto A Mano glass wine decanter (demonstrations of a wine glass and another shaped decanter are shown in Figure S8D in the Supporting Information).

Mild hydrostatic pressure is applied during the dipping process; this permits the LA to change shape freely to accommodate the fragile epidermal surface of fast-growing plants. To test the feasibility of hydroprinting on living plants, a growth experiment comparing three groups of bean sprout seedlings (pristine, immersed, and hydroprinted) was conducted (details are given in Figure S9 in the Supporting Information). As summarized in **Figure 4A**, new epicotyls and leaves are able to grow from the seedling, and the plants can grow in height in all three groups. The growth curve in terms of height of the hydroprinted group is very close to that of the pristine group as is that of both cotyledons and hypocotyls (Figure S10A, Supporting Information). This implies that both hydroprinting operation and LA patterns do not appreciably affect plant health and development. In addition, LAME was also transferred onto the surface of a peanut seedling before epicotyl and new leaves emerge, and the seedling remained healthy and grew for more than 2 months after printing (Figure S10B, Supporting Information). It means that this method is potential for long-term growing plants.

The stability and reliability of the LAME sensor were tested in Video S4 (Supporting Information). The electrical resistance of the sensor was measured when the rose petal was blown (simulating wind), bent, wetted (simulating rain), and exposed to moisture. The resistance value changed less than 1% for blown, wetted or moisture, and less than 3% for bending. The results show that the sensor has good stability and reliability under the influence of environmental stimulus.

To monitor physiological signals of plants, such as moisture content, we developed a dehydration sensor for lily and rose petals based on measuring the relative resistance changes of LAME (Figure 4B). When the petals are dehydrated, they shrink in volume and lead to shortened length and increased thickness of the LA sensor, resulting in decreased resistance with decreased relative moisture. Further, a curved LA can be used as a sensor for length detection. The relative length and relative resistance of the sensor in the growth process are shown in Figure 4C and in Figure S11 (Supporting Information). As bean sprouts grow from the bean-shaped cotyledons, hypocotyls elongate rapidly by cell enlargement. The upper part near the cotyledons visibly elongates but the lower part near the radicle remains almost unchanged (Figure S11, Supporting Information). The LAME remains conformably pinned on epidermis of the sprout and morphs with the dynamic stretching and deformation of the hypocotyl. Also, the length of the sensor increases by the same factor. Thus, cross-sectional area decreases while

the LA volume remains constant. Consequently, as shown in Figure 4C, the relative resistance has a square relationship with the relative length. Since bean sprouts exhibit phototropism, we employed LED–LAME on a bean sprout to manipulate its growth orientation by controlling LED emission in a black box (Figure 4D; and a comparison experiment in Figure S12 in the Supporting Information). The bending angle of the hypocotyl increases from 0° to over 180° as compared to that of the pristine control (Figure S12, Supporting Information). Further, an LED-integrated sprout was transplanted to a group of sprouts in the black box (Figure S13, Supporting Information). The LED-integrated sprout attracts and gathers the rest sprouts in the black box. Moreover, by selectively controlling LED emission on either side of the bean sprout cotyledon during the growth process, we manipulated the bean sprout to intertwine with a ladder (Figure 4E; Video S1, Supporting Information). During the sprout growth, the left LED emission induced sprout seedling growth toward the left while the right LED emission induced growth to the right. When the both LEDs are off, the seedling grows straight in the upward direction due the absence of phototropism. Moreover, the LED–LAME in Figure 4E covers both the cotyledon and hypocotyl. The cotyledon keeps almost same shape and size during the process, while hypocotyl stretches almost three times (left and right insets in Figure 4E), indicating a very useful combination of compliance, deformability, and functionality inherent in the LAME circuit.

### 3. Conclusion

In conclusion, using an innovative, gentle process of liquid alloy circuit printing on the highly micro-/nanostructured surfaces of the plant epidermis, we have developed new morphing electronics that can be directly printed onto complex and fragile 3D surfaces. Due to the excellent compliance, deformability, and functionality of liquid alloy circuits, it is suitable for sensing physiological signals arising in rapidly growing plants and can function as a biohybrid to influence plant morphological behavior. This study lays the foundation for a new form of biohybrid plant systems or robots and offers new tools for botany and precision agriculture research and development.

### 4. Experimental Section

**Hydroprinting:** First, the LA circuits were fabricated with masked printing<sup>[56]</sup> (Supporting Method and Figure S1, Supporting Information) or flexography printing reported previously.<sup>[60]</sup> A circular vinyl tape was

Inset images of LA ribbons on target substrate. C) Widths of transferred LA and PVA spacing between parallel ribbons at different transfer angles. D) Measured thickness of LA lines before (on PVA) and after hydroprinting (on silicone). E) Measured electrical resistance and width of LA lines before (on PVA) and after hydroprinting (on silicone). F) Arrays of varied liquid alloy and minimum line width and line spacing on hemisphere surfaces. G) An LED circuit with varied widths in shape of fractal tree on a hemisphere. H) An array of 6 × 6 LA squares printed on a silicone hemisphere. I) An annulus pattern with each ring equally spaced on the surface of a silicone hemisphere. The inset shows an optical photo at higher magnification. J) A multiline pattern containing angles from 10° to 90° with respect to the neighbor lines on the surface of a silicone hemisphere. The inset is a photograph of the pattern before hydroprinting (on PVA). K) A helical LA circuit of ≈1 mm width on a curvature-discontinuous glass sphere. L) A 3D LA ribbon wrapping around a resin-made column. Two panels show the both sides of the column. M) A connected circuit powering two LEDs on both sides of a PET film. Photos are taken front view, back view, and top view. N) An LA “HUST” logo printed on the inside wall of an Amadeo Fatto A Mano decanter. The inset is the enlarged view.



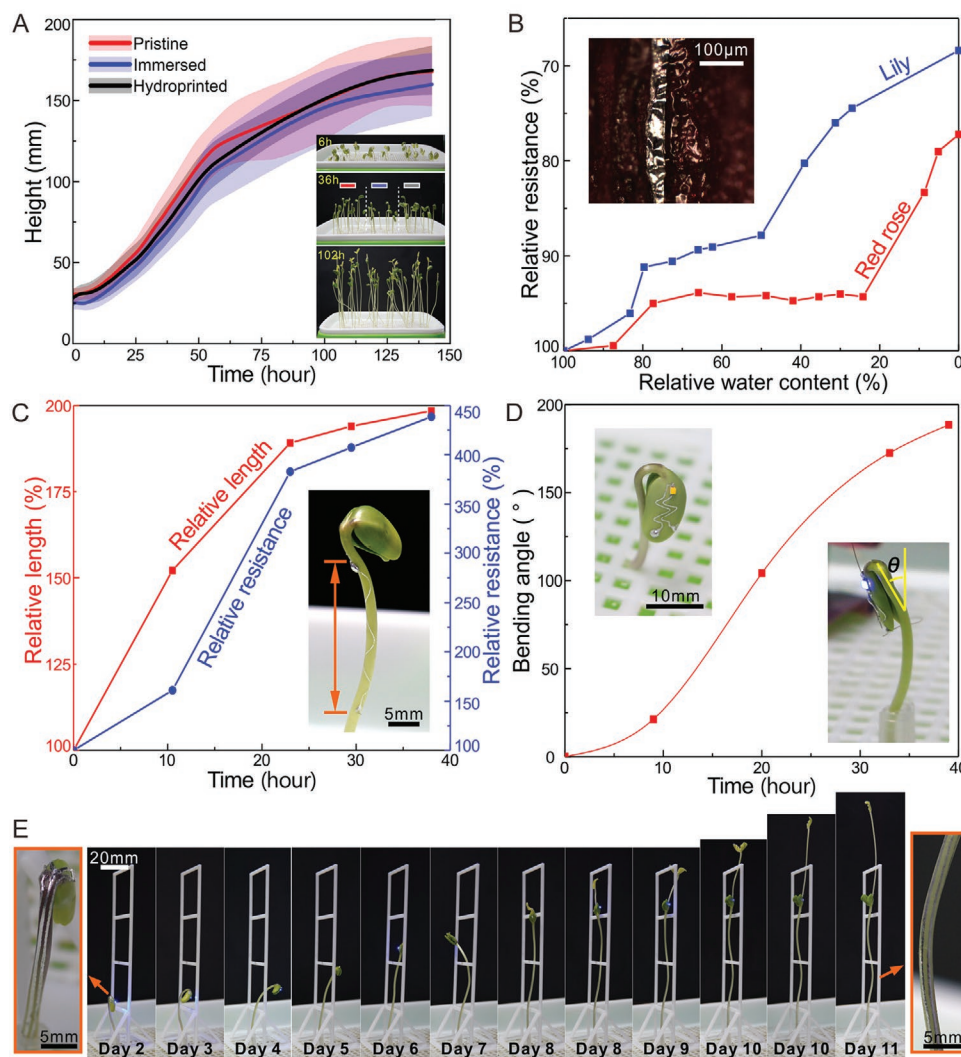


**Figure 4.** Plant growth monitoring and manipulation. A) Measured height of pristine, immersed, and hydroprinted bean sprouts during the growth process. The height is measured as the distance between the tip of cotyledons and the cultivating basin. B) The relative resistance of moisture sensors for lily and rose petals at various stages of dehydration. The inset shows an optical photo of LA morphology on a rose petal. C) The relative length of patterned sprout and the relative electrical resistance of length detection sensor as a function of growth time. D) The angle of the bean sprout bending as a function of time under LED illumination. E) Serial images of bean sprouts climbing a ladder. Orange border insets are images of the initial and the final LAME appearance on the seedling.

used as a frame encircling the patterned PVA film to keep the pattern in shape and prevent PVA film from expanding horizontally. During the hydroprinting process, the patterned PVA with a frame was placed onto the surface of water at 20°C for about 80 s to achieve thoroughly swollen (the placing time refers to the softening time in Figure S7D in the Supporting Information). Next, a target object or plant was aligned and dipped toward the LA pattern on the swollen PVA gel into the water. Finally, the object or plant was pulled out and immersed into a clean water vat for ≈30 min to dissolve residual PVA (Figure S2, Supporting Information). The estimation of processing time is listed in Table 1 and around 75 min was needed for a typical hydroprinting.

**Surface Characterizations:** The contact angles of LA on diverse surfaces were measured with a drop shape analysis equipment (DSA25, KRÜSS, Germany). The LA droplet was dropped via a syringe pump (PUMP 11 ELITE Nanomite, Harvard Apparatus, USA) at room temperature. For the dynamic contact angle measurement, the volume of LA droplet was increased or decreased at a speed of 6  $\mu\text{L min}^{-1}$ . For the static contact angle measurement, the volume of LA droplet was 4  $\mu\text{L}$ . The

inset photos in Figure 2A,C,D and in Figure S5 (Supporting Information) were captured by a camera attached to DSA25. An optical microscope (BA310MET-T, Motic, China) with a CCD camera (Moticam 3+, Motic, China) and an ultradepth 3D microscope (DSX 510, Olympus, Japan) were used to observe the LA patterns and microstructures as shown in Figure 2F and in Figures S4 and S6A (Supporting Information).

**Plants Experiments:** In the controlled experiment of plant health shown in Figure 4A and in Figures S9 and S10A (Supporting Information), homochronous bean sprouts were divided into three groups: the pristine, the immersed, and the hydroprinted. The pristine group was transplanted directly in the cultivating basin (only water was added). The hydroprinted group was operated by the whole process mentioned above including transferring and immersion. The immersed group was only immersed in water for 1 h. All of the three groups were transplanted in the same cultivating basin. The height is defined as the distance between the tip of cotyledons and the cultivating basin. Some sprouts fell sideways in the experiment, so only those remaining upright were counted in Figure 4A.

**Table 1.** Processing time estimation for a typical hydroprinting.

Processing steps	Time [min]
Pattern plotting <sup>a)</sup>	20
Mask tape lamination	2
UV laser ablation	2
Removal of the undesired pattern	2
LA spray deposition	2
Mask and paper substrate removal	2
PVA swelling <sup>b)</sup>	3
Transfer printing	2
Dissolve residual PVA gel <sup>c)</sup>	30
Drying	10
Total	75

<sup>a)</sup>Time varies according to the complexity of the designed pattern; <sup>b)</sup>This time refers to the softening time in Figure S7D (Supporting Information) and 3 min is sufficient for all experimental conditions; <sup>c)</sup>This time is estimated on the condition that the diameter of the pattern is less than 80 mm.

To speed up the water loss in the dehydration sensor experiment (Figures 1C and 4B), petals were heated at  $\approx 75^\circ\text{C}$  for 3 min between each measurement. A digital multimeter (34461A, Keysight Technologies, USA) and an analytical balance (Quintix224-1CN, Sartorius, Germany) were used to measure the resistance (Figure 4B,C) and weight (Figure 4B), respectively. To ensure good electrical contact between multimeter's probe tips and the sensor, the tips were coated with some LA before measurement.

The growth guiding experiment in Figures 1F and 4E was carried out in black box (Figure S15, Supporting Information) to avoid the interference from ambient light. Three wires were used to connect the two sides of LED circuits to the power, the middle one (red in Figure 1A,B-vii) for positive electrode, and the other two for each negative electrode (blue in Figure 1A,B-vii). The switch of LEDs was determined by the connection of power supply. The ladder structure was ablated with a laser marker and assembled by manually gluing. White, red, and blue LED lights were tested and all LED lights can enable the phototropism of plants. Blue LED was selected for use because of the good results achieved in previous pretests.

**Demonstrations on Inorganic Substrates:** The silicone hemisphere molds shown in Figure 3F–J were casted with PDMS (Sylgard 184, Dow Corning Corporation, USA), and all the patterns on PDMS are shown in Figure S16 (Supporting Information). Structures in Figure 3L were fabricated using a 3D printing method (commissioned to WeNext Tech, China). The pattern was divided into two parts (Figure S16, Supporting Information), and each part was subjected to a thorough hydroprinting process including transferring and dissolving. The double-sided circuit shown in Figure 3M was hydroprinted in a single process. The connecting patterns containing both sides of the circuit (Figure S16, Supporting Information) were spray-printed on a PVA film. Then an office used PET film was aligned vertically and dipped from the middle of the pattern into the water. After rinsing, two LEDs were placed on opposite sides and the whole circuit was sealed by silicone. Wine glass and decanters shown in Figure 3N and in Figure S8D (Supporting Information) were purchased from JD.com. The transfer method for inner wall pattern is shown in Figure S14 (Supporting Information). All the LED circuits shown were coated with LA in the footprints to ensure good electrical contact. The photographs were taken by two cameras (EOS 70D, Canon and Alpha 6000, Sony).

## Supporting Information

Supporting Information is available from the Wiley Online Library or from the author.

## Acknowledgements

J.J. and S.Z. contributed equally to this work. This work was partly financially supported by National Key R&D program of China (Grant No. 2017YFB1303100) and National Natural Science Foundation of China (Grant No. U1613204).

## Conflict of Interest

The authors declare no conflict of interest.

## Keywords

habit manipulation, high-surface-energy liquid-assisted pinning, hydroprinted liquid alloy circuits, liquid alloy behavior, morphing electronics, plant physiology monitors

Received: June 24, 2020

Published online:

- [1] J. P. Giraldo, H. Wu, G. M. Newkirk, S. Kruss, *Nat. Nanotechnol.* **2019**, *14*, 541.
- [2] R. C. Morrow, *HortScience* **2008**, *43*, 1947.
- [3] S.-Y. Kwak, M. H. Wong, T. T. S. Lew, G. Bisker, M. A. Lee, A. Kaplan, J. Dong, A. T. Liu, V. B. Koman, R. Sinclair, C. Hamann, M. S. Strano, *Annu. Rev. Anal. Chem.* **2017**, *10*, 113.
- [4] T. T. S. Lew, V. B. Koman, P. Gordiichuk, M. Park, M. S. Strano, *Adv. Mater. Technol.* **2020**, *5*, 1900657.
- [5] E. Stavrinidou, R. Gabrielsson, E. Gomez, X. Crispin, O. Nilsson, D. T. Simon, M. Berggren, *Sci. Adv.* **2015**, *1*, e1501136.
- [6] E. Stavrinidou, R. Gabrielsson, K. P. R. Nilsson, S. K. Singh, J. F. Franco-Gonzalez, A. V. Volkov, M. P. Jonsson, A. Grimoldi, M. Elgland, I. V. Zozoulenko, D. T. Simon, M. Berggren, *Proc. Natl. Acad. Sci. USA* **2017**, *114*, 2807.
- [7] L. Angelini, M. Caon, S. Caparrotta, O. A. Khaled, E. Mugellini, in *Proceedings of the 2016 ACM International Joint Conference on Pervasive and Ubiquitous Computing: Adjunct*, Association For Computing Machinery, New York, NY, USA **2016**, pp. 1001–1009.
- [8] J. P. Giraldo, M. P. Landry, S. M. Faltermeier, T. P. McNicholas, N. M. Iverson, A. A. Boghossian, N. F. Reuel, A. J. Hilmer, F. Sen, J. A. Brew, M. S. Strano, *Nat. Mater.* **2014**, *13*, 400.
- [9] S. Y. Kwak, J. P. Giraldo, M. H. Wong, V. B. Koman, T. T. S. Lew, J. Ell, M. C. Weidman, R. M. Sinclair, M. P. Landry, W. A. Tisdale, M. S. Strano, *Nano Lett.* **2017**, *17*, 7951.
- [10] S. K. Chatterjee, S. Ghosh, S. Das, V. Manzella, A. Vitaletti, E. Masi, L. Santopolo, S. Mancuso, K. Maharatna, *Measurement* **2014**, *53*, 101.
- [11] S. Oren, H. Ceylan, P. S. Schnable, L. Dong, *Adv. Mater. Technol.* **2017**, *2*, 1700223.
- [12] J. M. Nassar, S. M. Khan, D. R. Villalva, M. M. Nour, A. S. Almuslem, M. M. Hussain, *npj Flexible Electron.* **2018**, *2*, 24.
- [13] F. Meder, I. Must, A. Sadeghi, A. Mondini, C. Filippeschi, L. Beccai, V. Mattoli, P. Pingue, B. Mazzolai, *Adv. Funct. Mater.* **2018**, *28*, 1806689.
- [14] Y. Jie, X. Jia, J. Zou, Y. Chen, N. Wang, Z. L. Wang, X. Cao, *Adv. Energy Mater.* **2018**, *8*, 1703133.
- [15] D.-H. Kim, N. Lu, R. Ma, Y.-S. Kim, R.-H. Kim, S. Wang, J. Wu, S. M. Won, H. Tao, A. Islam, K. J. Yu, T.-i. Kim, R. Chowdhury, M. Ying, L. Xu, M. Li, H.-J. Chung, H. Keum, M. McCormick, P. Liu, Y.-W. Zhang, F. G. Omenetto, Y. Huang, T. Coleman, J. A. Rogers, *Science* **2011**, *333*, 838.

- [16] W.-H. Yeo, Y.-S. Kim, J. Lee, A. Ameen, L. Shi, M. Li, S. Wang, R. Ma, S. H. Jin, Z. Kang, Y. Huang, J. A. Rogers, *Adv. Mater.* **2013**, 25, 2773.
- [17] T. Q. Trung, N.-E. Lee, *Adv. Mater.* **2016**, 28, 4338.
- [18] Y. Hwang, S. Yoo, N. Lim, S. M. Kang, H. Yoo, J. Kim, Y. Hyun, G. Y. Jung, H. C. Ko, *ACS Nano* **2020**, 14, 118.
- [19] J. Park, Y. Lee, H. Lee, H. Ko, *ACS Nano* **2020**, 14, 12.
- [20] R. C. Webb, A. P. Bonifas, A. Behnaz, Y. Zhang, K. J. Yu, H. Cheng, M. Shi, Z. Bian, Z. Liu, Y.-S. Kim, *Nat. Mater.* **2013**, 12, 938.
- [21] J. Jeon, H.-B.-R. Lee, Z. Bao, *Adv. Mater.* **2013**, 25, 850.
- [22] C. Dagdeviren, Y. Su, P. Joe, R. Yona, Y. Liu, Y.-S. Kim, Y. Huang, A. R. Damadoran, J. Xia, L. W. Martin, Y. Huang, J. A. Rogers, *Nat. Commun.* **2014**, 5, 4496.
- [23] C.-L. Choong, M.-B. Shim, B.-S. Lee, S. Jeon, D.-S. Ko, T.-H. Kang, J. Bae, S. H. Lee, K.-E. Byun, J. Im, Y. J. Jeong, C. E. Park, J.-J. Park, U. I. Chung, *Adv. Mater.* **2014**, 26, 3451.
- [24] H. Li, Y. Xu, X. Li, Y. Chen, Y. Jiang, C. Zhang, B. Lu, J. Wang, Y. Ma, Y. Chen, Y. Huang, M. Ding, H. Su, G. Song, Y. Luo, X. Feng, *Adv. Healthcare Mater.* **2017**, 6, 1601013.
- [25] A. J. Bandodkar, W. Jia, C. Yardimci, X. Wang, J. Ramirez, J. Wang, *Anal. Chem.* **2015**, 87, 394.
- [26] Y. Chen, S. Lu, S. Zhang, Y. Li, Z. Qu, Y. Chen, B. Lu, X. Wang, X. Feng, *Sci. Adv.* **2017**, 3, e1701629.
- [27] J.-W. Jeong, W.-H. Yeo, A. Akhtar, J. J. S. Norton, Y.-J. Kwack, S. Li, S.-Y. Jung, Y. Su, W. Lee, J. Xia, H. Cheng, Y. Huang, W.-S. Choi, T. Bretl, J. A. Rogers, *Adv. Mater.* **2013**, 25, 6839.
- [28] J. J. Park, W. J. Hyun, S. C. Mun, Y. T. Park, O. O. Park, *ACS Appl. Mater. Interfaces* **2015**, 7, 6317.
- [29] C. Yan, J. Wang, W. Kang, M. Cui, X. Wang, C. Y. Foo, K. J. Chee, P. S. Lee, *Adv. Mater.* **2014**, 26, 2022.
- [30] S. H. Jeong, S. Zhang, K. Hjort, J. Hilborn, Z. G. Wu, *Adv. Mater.* **2016**, 28, 5765.
- [31] J. Park, M. Kim, Y. Lee, H. S. Lee, H. Ko, *Sci. Adv.* **2015**, 1, e1500661.
- [32] A. Chortos, J. Liu, Z. Bao, *Nat. Mater.* **2016**, 15, 937.
- [33] Q. Hua, J. Sun, H. Liu, R. Bao, R. Yu, J. Zhai, C. Pan, Z. L. Wang, *Nat. Commun.* **2018**, 9, 244.
- [34] S. Wang, J. Xu, W. Wang, G.-J. N. Wang, R. Rastak, F. Molina-Lopez, J. W. Chung, S. Niu, V. R. Feig, J. Lopez, T. Lei, S.-K. Kwon, Y. Kim, A. M. Foudeh, A. Ehrlich, A. Gasperini, Y. Yun, B. Murmann, J. B.-H. Tok, Z. Bao, *Nature* **2018**, 555, 83.
- [35] Y. Lee, J. Park, S. Cho, Y. E. Shin, H. Lee, J. Kim, J. Myoung, S. Cho, S. Kang, C. Baig, H. Ko, *ACS Nano* **2018**, 12, 4045.
- [36] X. Yu, Z. Xie, Y. Yu, J. Lee, A. Vazquez-Guardado, H. Luan, J. Ruban, X. Ning, A. Akhtar, D. Li, B. Ji, Y. Liu, R. Sun, J. Cao, Q. Huo, Y. Zhong, C. Lee, S. Kim, P. Gutruf, C. Zhang, Y. Xue, Q. Guo, A. Chempakasseril, P. Tian, W. Lu, J. Jeong, Y. Yu, J. Cornman, C. Tan, B. Kim, K. Lee, X. Feng, Y. Huang, J. A. Rogers, *Nature* **2019**, 575, 473.
- [37] J. J. Kim, L. K. Allison, T. L. Andrew, *Sci. Adv.* **2019**, 5, eaaw0463.
- [38] J. Li, presented at 2019 AICHE Annu. Meet., Orlando, USA, November **2019**.
- [39] J. Li, presented at 2019 Mater. Res. Soc. Fall Meet. Exhib., Boston, USA, December, **2019**.
- [40] Y. Liu, J. Li, S. Song, J. Kang, Y. Tsao, S. Chen, V. Mottini, K. McConnell, W. Xu, Y.-Q. Zheng, J. B.-H. Tok, P. M. George, Z. Bao, *Nat. Biotechnol.* <https://doi.org/10.1038/s41587-020-0495-2>.
- [41] C. Müller, M. Riederer, *J. Chem. Ecol.* **2005**, 31, 2621.
- [42] K. Koch, W. Barthlott, *Philos. Trans. R. Soc., A* **2009**, 367, 1487.
- [43] R. C. Chiechi, E. A. Weiss, M. D. Dickey, G. M. Whitesides, *Angew. Chem., Int. Ed.* **2008**, 47, 142.
- [44] M. D. Dickey, *ACS Appl. Mater. Interfaces* **2014**, 6, 18369.
- [45] S. Cheng, Z. Wu, *Lab Chip* **2012**, 12, 2782.
- [46] E. Palleau, S. Reece, S. C. Desai, M. E. Smith, M. D. Dickey, *Adv. Mater.* **2013**, 25, 1589.
- [47] X. Wang, J. Liu, *Micromachines* **2016**, 7, 206.
- [48] M. D. Dickey, *Adv. Mater.* **2017**, 29, 1606425.
- [49] N. Kazem, T. Hellebrekers, C. Majidi, *Adv. Mater.* **2017**, 29, 1605985.
- [50] Y. Zheng, Z. He, Y. Gao, J. Liu, *Sci. Rep.* **2013**, 3, 1786.
- [51] J. W. Boley, E. L. White, G. T.-C. Chiu, R. K. Kramer, *Adv. Funct. Mater.* **2014**, 24, 3501.
- [52] Y. Zheng, Z.-Z. He, J. Yang, J. Liu, *Sci. Rep.* **2015**, 4, 4588.
- [53] Y. Zheng, Q. Zhang, J. Liu, *AIP Adv.* **2013**, 3, 112117.
- [54] S. H. Jeong, A. Hagman, K. Hjort, M. Jobs, J. Sundqvist, Z. Wu, *Lab Chip* **2012**, 12, 4657.
- [55] R. K. Kramer, C. Majidi, R. J. Wood, *Adv. Funct. Mater.* **2013**, 23, 5292.
- [56] S. H. Jeong, K. Hjort, Z. Wu, *Sci. Rep.* **2015**, 5, 8419.
- [57] C. Ladd, J. So, J. Muth, M. D. Dickey, *Adv. Mater.* **2013**, 25, 5081.
- [58] Y. Yu, F. Liu, R. Zhang, J. Liu, *Adv. Mater. Technol.* **2017**, 2, 1700173.
- [59] Y. He, L. Zhou, J. Zhan, Q. Gao, J. Fu, C. Xie, H. Zhao, Y. Liu, *3D Print. Addit. Manuf.* **2018**, 5, 195.
- [60] S. Zhang, B. Wang, J. Jiang, K. Wu, C. F. Guo, Z. Wu, *ACS Appl. Mater. Interfaces* **2019**, 11, 7148.
- [61] Y. Zhang, C. Yin, C. Zheng, K. Zhou, *ACM Trans. Graphics* **2015**, 34, 131.
- [62] B. Le Borgne, O. De Sagazan, S. Crand, E. Jacques, M. Harnois, *ACS Appl. Mater. Interfaces* **2017**, 9, 29424.
- [63] B. LeBorgne, S. Liu, X. Morvan, S. Crand, R. A. Sporea, N. Lu, M. Harnois, *Adv. Mater. Technol.* **2019**, 4, 1800600.
- [64] G. Saada, M. Layani, A. Chervonousky, S. Magdassi, *Adv. Mater. Technol.* **2017**, 2, 1600289.
- [65] D. Groeger, J. Steimle, *Proc. ACM Interact. Mob. Wearable Ubiquitous Technol.* **2018**, 1, 134.
- [66] L. W. T. Ng, X. Zhu, G. Hu, N. Macadam, D. Um, T. C. Wu, F. Le Moal, C. Jones, T. Hasan, *Adv. Funct. Mater.* **2019**, 29, 1807933.
- [67] P. A. Lopes, H. Paisana, A. T. De Almeida, C. Majidi, M. Tavakoli, *ACS Appl. Mater. Interfaces* **2018**, 10, 38760.
- [68] I. D. Joshipura, H. R. Ayers, G. A. Castillo, C. Ladd, C. E. Tabor, J. J. Adams, M. D. Dickey, *ACS Appl. Mater. Interfaces* **2018**, 10, 44686.
- [69] M. D. Dickey, R. C. Chiechi, R. J. Larsen, E. A. Weiss, D. A. Weitz, G. M. Whitesides, *Adv. Funct. Mater.* **2008**, 18, 1097.